

Underwater adhesion of abalone: The role of van der Waals and capillary forces

A.Y.M. Lin^{d,*}, R. Brunner^{a,b}, P.Y. Chen^d, F.E. Talke^{a,c}, M.A. Meyers^{a,b,d}

^a Department of Mechanical and Aerospace Engineering, University of California, San Diego, La Jolla, CA 92093, USA

^b Department of Nanoengineering, University of California, San Diego, La Jolla, CA 92093, USA

^c Center for Magnetic Recording Research, University of California, San Diego, La Jolla, CA 92093, USA

^d Materials Science and Engineering Program, University of California, San Diego, La Jolla, CA 92093, USA

Received 21 October 2008; received in revised form 24 April 2009; accepted 12 May 2009

Available online 6 June 2009

Abstract

The observation of the pedal foot of the red abalone *Haliotis rufescens* reveals the presence of micrometer-scaled setae terminating in nanometer-sized cylindrical fibrils, with some resemblance to those found on the gecko foot. Atomic force microscopy (AFM) pull-off force measurements on a single seta are compared with theoretical estimates for van der Waals attraction obtained through the Johnson–Kendall–Roberts (JKR) equation, approximately 600 nN, and show agreement. The use of the JKR equation is justified through an analysis of the shape of the fibril extremities (parabolic) as well as their diameter (~200 nm). Measurements under varying humidity conditions indicate that additional capillary interactions play a role, since the pull-off force increases with humidity. It is proposed that both van der Waals and capillary forces play a role in the attachment mechanism of *H. rufescens*, effectively enabling suction to reach its theoretical limit. Bulk pull-off force measurements on entire live animals yield an average detachment stress of 115 kPa, consistent with theoretical estimates. The setae and nanoscale fibril terminations enable compliance to surfaces with a variety of roughnesses, effectively sealing the interface, in addition to providing capillary and van der Waals forces.

© 2009 Acta Materialia Inc. Published by Elsevier Ltd. All rights reserved.

Keywords: Abalone foot; Underwater adhesion; Van der Waals forces

1. Introduction

Numerous organisms have the ability to functionally adhere to surfaces. Geckos, for example, have received significant attention for their ability to climb smooth vertical surfaces employing van der Waals and capillary forces generated by nanoscaled fibrils on their feet [1–4]. Additionally, similar adhesive mechanisms have been found in a variety of other land animals, such as tree frogs [5,6] and insects [7]. Barnes [6] classifies attachment devices in animals into interlocking, friction and bonding. Interlocking is the mechanism by which felines climb trees. This is a strictly mechanical process and can be accomplished by

penetrating the surface with sharp claws. Friction consists of the microinterlocking of the surfaces because of their roughness and intermolecular forces between materials and requires an angle that is below 90°. Bonding involves the formation of bonds between the animal and the surface and has three possible mechanisms acting separately or together: wet adhesion (capillarity), dry adhesion (van der Waals) and suction (through reduced internal pressure).

The reusability and versatility of natural attachment devices on a variety of surfaces under varying conditions [8,9] has an efficiency not yet matched in modern technology. Thus, a number of efforts to synthetically mimic these natural attachment devices are currently under way (e.g. [10–23]). Of special significance is the recent development of a gecko-inspired tissue adhesive for biomedical applica-

* Corresponding author. Tel.: +1 858 349 1399; fax: +1 858 822 1129.
E-mail address: albertlin22@yahoo.com (A.Y.M. Lin).

tions by Langer and co-workers [17]. They demonstrated that gecko-inspired arrays of pillars of polyglycerol sebacate acrylate provided attachment under water. This tape is proposed as a biodegradable polymer adhesive to tissue. The adhesion was tested in vitro to porcine intestine and in vivo to rat abdominal muscle. Carbon nanotube arrays have also been proposed to form fibrillar arrays and have self-cleaning properties due to an extreme hydrophobicity [16]. The effects of angled fibrillar attachments have also been investigated and it was demonstrated to have an important bearing. The angular array of fibrils has been biomimicked by Yao et al. [19] using polydimethylsiloxane arrays and by Lee et al. [20] using polypropylene arrays. Greiner et al. [21] and del Campo et al. [22] produced hierarchically structured polydimethylsiloxane with two scales and explored its advantages.

Complex fibrous hyperstructures, which vary in hierarchy, dimensions and material properties, are the key to these devices [23,24]. The structures have been found to produce intimate contacts with surfaces creating interactions at the molecular level. To date, this specific mechanism in nature has only been observed in land species. Marine organisms such as mussels, octopi and sea stars have been found to employ alternative mechanisms for adhesion, such as suction or quick-acting protein-based glues [25–29].

This article provides evidence that van der Waals forces, acting in combination with capillary forces as a result of nanofibrils, may contribute to the strong adhesion exhibited by a marine species, the abalone. The scope of applications for future synthetic nanofibril attachment devices thus broadens to include use in wet environments, opening the door to applications ranging from marine engineering to biomedical sciences.

2. Experimental methods

In vivo macromechanical tests of the bulk pull-off force of adult abalone feet were performed. The tests were conducted on live abalone with an average foot area of $5.5 \times 10^{-3} \text{ m}^2$. The animals were held in an open water facility in the Hubbs Hall Laboratory at the Scripps Institute of Oceanography, La Jolla, CA prior to testing. A three-pronged steel jaw was used to clamp the abalone shells; its other end was attached to a cable that was fed through a pulley to a platform on which weights were incrementally placed. The detachment force was measured on a smooth, painted tank in which the abalone had been held for over a year before testing.

For SEM characterization, small pieces of abalone foot ($\sim 5 \text{ mm} \times 5 \text{ mm} \times 3 \text{ mm}$) were carefully cut without altering the surface. Samples were dried using the critical point drying procedure, with the structure maintained throughout the process. They were then mounted on aluminum sample holders and coated with a thin layer of gold in a sputter coater. A field emission scanning electron microscope equipped for electron-dispersive spectroscopy

(FEI-XL30, FEI Company, OR, USA) was used. In order to get high-magnification and high-resolution images, a high vacuum mode was used instead of the environmental mode.

For testing with an atomic force microscope (AFM), the method developed by Huber et al. for use with individual gecko setae was used [8,30]. Samples of tissue from the foot of the abalone were dried by critical point drying, allowing preservation of the sample structure. Single abalone setae were attached to AFM cantilevers using an optical microscope and micrometer stage. Each seta was glued to the end of a contact mode cantilever (Veeco NP-20) with a spring constant of 0.58 N m^{-1} .

The sample preparation procedure for atomic force microscopy testing is outlined next. First, the AFM tip was brought into contact with the tip of a needle covered with ultraviolet (UV)-hardening glue, allowing the glue to cover the tip of the cantilever. Then the tip of the cantilever was positioned over a single seta on the abalone foot tissue. When the seta was in contact with the cantilever tip, UV light was used to harden the glue, thereby producing a firm connection between the seta and the cantilever tip. Finally, the seta was sheared off the foot tissue.

The pull-off force for a single seta was measured perpendicular to a hydrophilic (silicon oxide) and a hydrophobic (carbon coated thin film disks) substrate. The water contact angle was determined to be 48° for the hydrophilic material and 98° for the hydrophobic material. The roughness average (R_a) of the hydrophilic material was 0.8 nm and that of the hydrophobic material was 0.4 nm. The AFM was placed in a sealed enclosure to allow controlled humidity variation within the testing environment. Dry nitrogen was introduced in the AFM chamber to reduce the humidity, which was measured by a hydroscope.

3. Results and discussion

3.1. Abalone foot characterization

Fig. 1A shows an abalone supporting its own weight via a single contact point (a human finger). The size of a pedal foot of red abalone (*Haliotis rufescens*) is shown in Fig. 1B (scale in mm). The dark pedal folds, spaced approximately 0.5 mm apart, are the source of locomotion waves used in transportation [31,32]. Fig. 1C shows a high-magnification scanning electron microscopy (SEM) image of the cross-section of the sole tissue. Folds can be seen clearly as the way in which the surface area of the foot can expand and contract, allowing an increase or decrease in contact surface area and providing the mechanism for the propagation of waves on the ventral surface of the pedal muscle [31]. At higher magnification, Fig. 2A shows setae lining the outer surface of the tissue with a thickness of $\sim 2 \mu\text{m}$. At their extremities (Fig. 2B), the setae separate into nanoscaled fibrils with rounded ends, averaging 200 nm in diameter and uniaxially aligned perpendicular to the plane of the foot tissue.

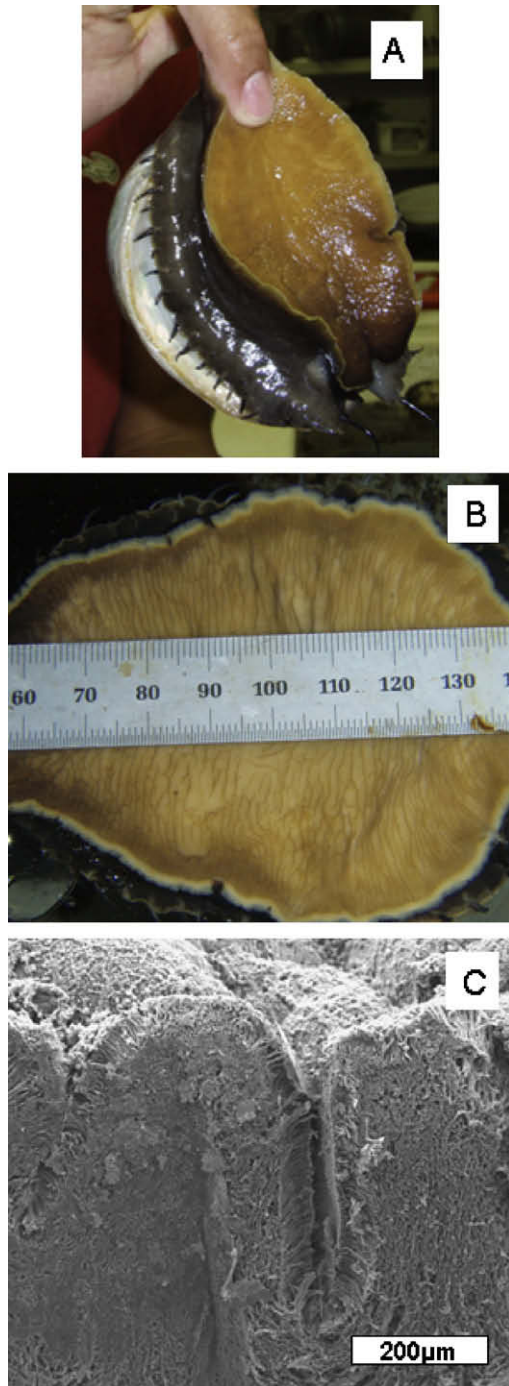


Fig. 1. Optical images of abalone foot: (A) an abalone sticking to a human finger using only a fraction of its foot; (B) an abalone foot attached to a glass plate, showing its dimensions (scale in mm) and (C) cross-section of the foot pedal. The surface of the foot can expand and contract through folds.

The angle of alignment of setae and nanofibrils relative to the attached substrate is critical in the attachment process. Fig. 3A provides an SEM image of a cleaved section of pedal foot tissue at the interface between the tissue and an attached piece of kelp. The kelp extends downward from the upper right-hand quadrant of the image, while setae can be observed to extend upward perpendicular to

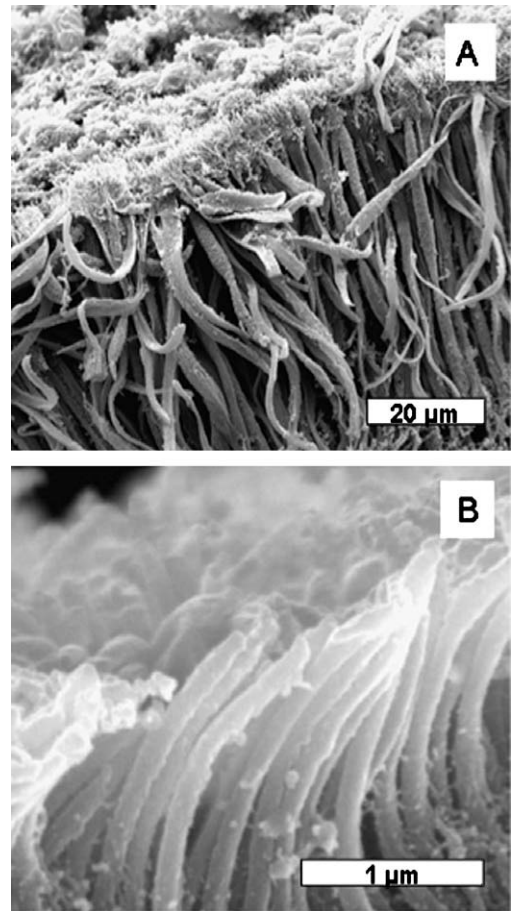


Fig. 2. SEM images showing detailed nature of foot surface with fibers terminating in nanofibrils: (A) ventral side of tissue consisting of fibers 100 μm in length and 2 μm in diameter, called setae and (B) nanofibrils with ~200 nm diameters.

the interface. Fig. 3B shows the alignment of the nanofibrils as they extend outward from the setae; strong uniaxial alignment throughout the various levels of structural hierarchy can be observed.

3.2. Analysis of shape of fibril extremities

Fig. 4 shows a close-up of the fibril extremities. They have a rounded shape with a diameter of approximately 200 nm. Fibril extremities have been previously analyzed by Gao and Yao [33,34], who showed this shape to have an important effect on the van der Waals forces. They represented the extremity shape by the two-dimensional mathematical power law equation (since there is axial symmetry to the shape):

$$z(r) = \frac{r^n}{nR^{n-1}} \quad (1)$$

where $z(r)$ represents the curve, r is the radial distance from the axis of symmetry, R is a characteristic length and n is a parameter ($n > 0$). Fig. 5A shows the predicted shapes as a function of n , which varies from 1 to 8. For $n = 1$, the tip is conical; as n increases, the tip flattens. Several extremity

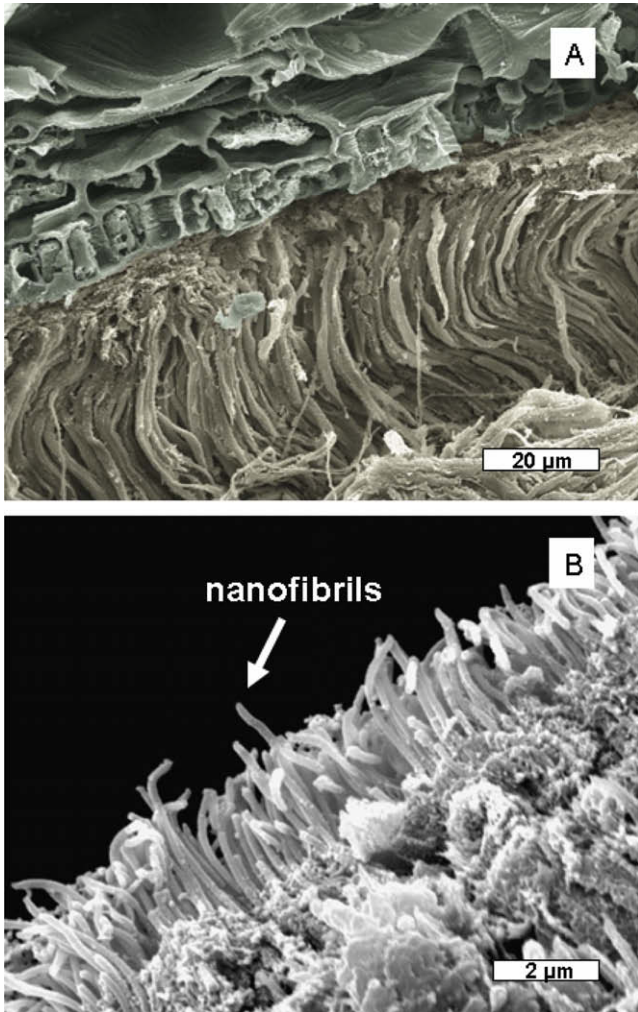


Fig. 3. SEM images of: (A) the interface between the pedal foot tissue and an attached substrate (kelp), with the alignment of the setae perpendicular to the substrate and (B) cross-section of the foot tissue in high magnification showing the uniaxial alignment between neighbouring nanofibrils.

profiles traced from six fibrils observed by SEM are shown in Fig. 5B. Table 1 shows the best fit parameter n . It fluctuates from 1.93 to 2.48, with an average of 2.13. This is close to $n = 2$, a value for which Eq. (1) reduces to:

$$z(r) = \frac{1}{2R} r^2 \quad (2)$$

This is a parabola.

The three best equations for contact mechanics stem from the Johnson–Kendall–Roberts (JKR) [35], Derjaguin–Muller–Toporov [36] and Maugis–Dugdale [37,38] models. Yao and Gao [34] compare the three theories and develop the general expression of the pull-off force, P_c , for an extremity shape given by the power function (Eq. (1)):

$$P_c = \sqrt{2\pi} \left(\frac{2n-1}{n+1} \right) \left[\frac{3\Gamma(1/2+n/2)}{\sqrt{2}\Gamma(1+n/2)} \right]^{\frac{3}{2n-1}} \times E^{n/(2n-1)} R^{3(n-1)/(2n-1)} \Delta\gamma^{(n+1)/(2n-1)} \quad (3)$$

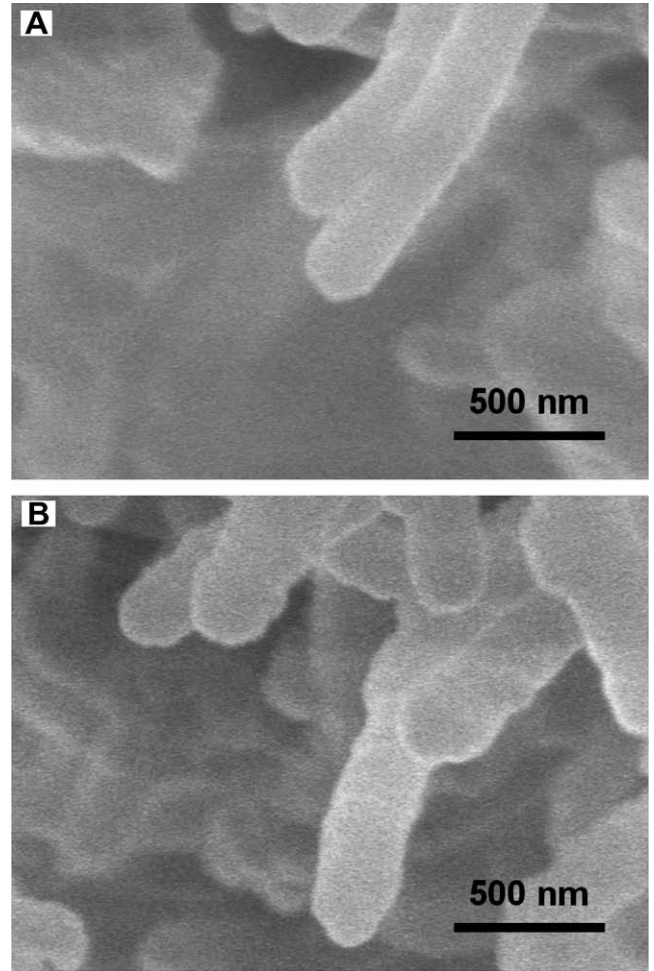


Fig. 4. High-magnification field-emission SEM images of abalone fibrils showing the diameter is ~ 200 nm.

where E' is the biaxial elastic modulus ($=E/(1-\nu^2)$), $\Delta\gamma$ is the surface energy and Γ is the gamma function. For $n = 2$, the elastic modulus term disappears and Eq. (3) reduces itself to:

$$P_c = \frac{3}{2} \pi R \Delta\gamma \quad (4)$$

since

$$\Gamma(1/2) = \sqrt{\pi} \quad \text{and} \quad \Gamma(3/2) = \frac{\sqrt{\pi}}{2}$$

This is the JKR form of the pull-off force equation.

3.3. Theoretical approximation of van der Waals forces in the abalone foot

In the case of the abalone, we observe from Fig. 2B the presence of roughly 25 effective nanofibrils per μm^2 , giving an areal density of 2.5×10^{13} nanofibrils m^{-2} . Thus, an abalone with an area of 5.5×10^{-3} m^2 contains approximately 1.38×10^{11} nanofibrils. This value can be used to predict the pull-off force of the entire abalone foot assuming that the molecular interaction between the nanofibrils

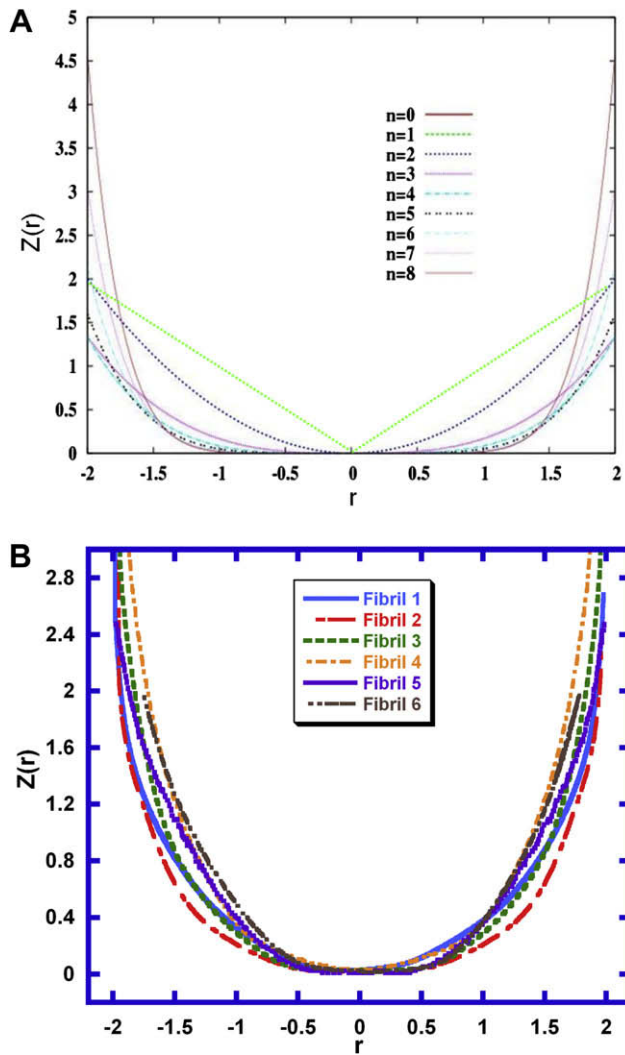


Fig. 5. (A) Power law surfaces $z = r^n/nR^n$. The parabolic case $n = 2$ fits the contact surface of abalone fibrils best and (B) the surface geometry of several abalone fibrils.

Table 1
Fibril extremity parameters from the Yao–Gao [33,34] equation (power law surface).

	n	Asymmetry (%)
1	2.22	0.18
2	2.48	0.41
3	2.18	0.35
4	1.94	0.26
5	2.05	0.17
6	1.93	0.21
Average	2.13 ± 0.21	

and a substrate is the primary mechanism of adhesion. It is shown in Section 3.2 that the JKR theory [35] can be applied to the fibril extremities of the abalone foot.

To estimate the contribution of the van der Waals interaction, the interfacial energy can be calculated as:

$$\Delta\gamma = \frac{A}{24\pi D_0^2} \quad (5)$$

where A is the material-dependent Hamaker constant and D_0 is the cutoff distance. $D_0 = 0.165$ nm is a universal constant and can be used for most materials [39]. The Hamaker constants for polymeric materials are 4.5×10^{-2} J for PDMS [40], 6.1×10^{-2} J for polyester [40], 6.6×10^{-2} J for polystyrene [39] and 7.8×10^{-2} J for polyvinyl chloride [39]. Using an average of 6×10^{-2} J for the Hamaker constant A and 0.165 nm for D_0 , the interfacial energy $\Delta\gamma$ is 30 mJ m $^{-2}$. The tip has parabolic geometry, and the radius is measured to be 75 nm from Fig. 4. Using Eq. (4), the contact force of a single nanofibril can be calculated to be 10 nN, which is in good agreement with the pull-off force of individual gecko spatulae by AFM [30]. The pull-off force for a seta with $2.5 \mu\text{m}^2$ tip area (containing 60 nanofibrils) is 600 nN. The total attractive force due to van der Waals interactions along the foot of a typical abalone can be approximated by multiplying the force per nanofibril by the total number of nanofibrils. For a foot area of 5.5×10^{-3} m 2 one obtains a total force of 1.32 kN, corresponding to a stress of approximately, 240 kPa.

3.4. Force estimation of a single seta during perpendicular pull-off using an AFM

AFM pull-off force measurements using force–distance curves of a single seta were performed using an approach developed by Huber et al. [8,30] for the gecko foot. As seen from Fig. 6, no glue was attached to the cantilever beam. The measurements were done with the same seta. Fig. 7 shows a typical force–distance measurement used to determine the pull-off force. First, the seta was brought into close proximity to the testing surface. This distance was reduced (points A and B) until the AFM tip “snaps” into contact (point B). Further movement of the AFM tip towards the surface causes perpendicular preloading of the seta onto the silicone substrate (point C). After reach-

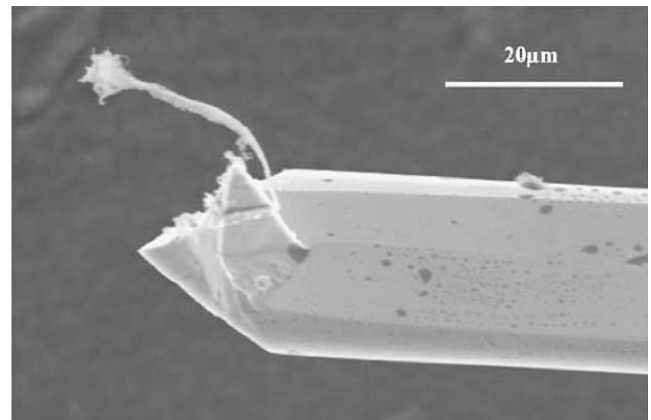


Fig. 6. Single abalone seta terminating in a nanofibril bundle attached to an AFM cantilever tip.

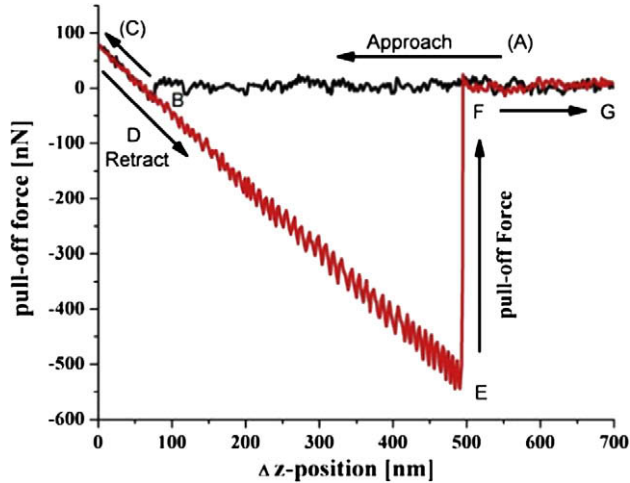


Fig. 7. Force–distance measurement using AFM to determine the pull-off force.

ing point C, the tip was retracted from the surface until the pull-off force exceeds the adhesion force between the seta and the surface (point E). At that point, the AFM tip separates from the surface (line E and F). The cantilever deflection between E and F can provide a quantitative measure for the adhesion force at the interface. The measurements were conducted for values between 10% and 67% humidity to study its effect on possible capillary forces.

Fig. 8 shows that the pull-off force increases with increasing humidity for the hydrophilic material while for the hydrophobic material it remains constant. In the case of the hydrophobic material, the average pull-off force was determined to be 294 nN, which remained constant under varying humidity. The number of nanofibrils on a single seta in contact with the surface was estimated to be 60; this corresponds to an adhesion force of approximately

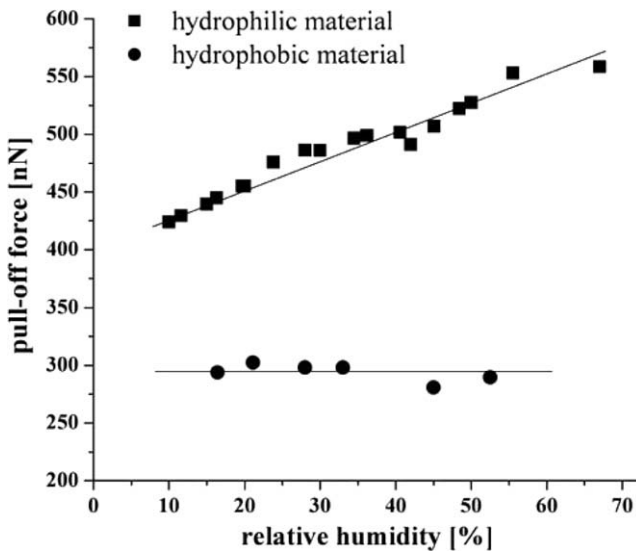


Fig. 8. The pull-off force for a single seta on a hydrophilic material (silicon oxide) and a hydrophobic material (carbon coated magnetic disk) as a function of humidity.

5 nN per nanofibril. This estimate is in good agreement with the theoretical results of 10 nN calculated using the JKR equation (Section 3.3).

When the seta was tested on a hydrophilic substrate at a relative humidity of 10%, the pull-off force was observed to be 424 nN. This represents an increased force of 130 nN relative to the test on the hydrophobic substrate, which can be partially explained by the difference in the surface energies of the two substrates (20 and 55.5 mJ m⁻² for the disk and silicon oxide, respectively). The increase in pull-off force is not as high as one would predict from the difference in surface energy and therefore other factors may be playing a role. However, raising the relative humidity to 67% resulted in an additional increase in pull-off force to 558 nN. Similar to predictions by Autumn et al. [3] and the work by Huber et al. [8] for the gecko foot, this shows evidence of capillary interactions. The influence of a meniscus fluid between a fiber and a substrate is increasingly significant with decreased liquid–surface contact angle, i.e. a hydrophilic substrate should favor more capillary interactions than a hydrophobic one. This is clearly seen in Fig. 8.

3.5. Bulk mechanical testing of pull-off force of the abalone foot

Seven abalone specimens were tested, providing an average pull-off stress of 115 kPa with a standard deviation of 19 kPa. This is of the same order as the theoretical stress of 240 kPa calculated from van der Waals forces. It should be clarified that it is not proposed that this is the sole result of van der Waals forces, as will be shown in Section 3.6. Fig. 9 shows the results of the individual tests plotted in

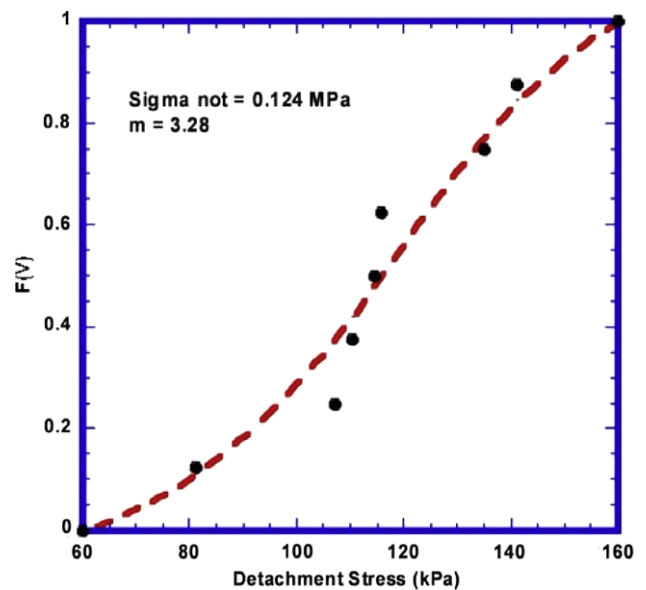


Fig. 9. Cumulative distribution (failure probability) as a function of perpendicular pull-off stresses of the entire abalone (Weibull distribution superimposed on experimental results).

a Weibull fashion. The distribution of pull-off stresses is seen.

3.6. Attachment hierarchy

The characterization of the abalone foot pedal and the mechanical tests suggest that the three mechanisms (van der Waals, capillarity and suction) act cooperatively (and perhaps synergistically). The attachment forces generated by suction are explained schematically in Fig. 10A. The detachment force F_d is equal to:

$$F_d = PA \quad (6)$$

where P is the pressure and A is the projected area of the abalone foot on the plane of the surface of attachment. Assuming that the effect of the water column is negligible, i.e. $P = P_{\text{atm}}$, we obtain the mean attachment stress as,

$$\sigma_d = \frac{F_d}{A} = P_{\text{atm}} = 101 \text{ kPa} \quad (7)$$

Figs. 10B and 10C show schematically how the three mechanisms can operate cooperatively to create attachment stress of the same order of magnitude as the theoretical suction stress. The setae and nanofibrils maintain intimate contact with any irregular surface, closing any possible channels and impeding water penetration. The pressure at the interface, P_0 , is equal to P_{atm} when no external detachment force is applied. As F_d increases, P_0

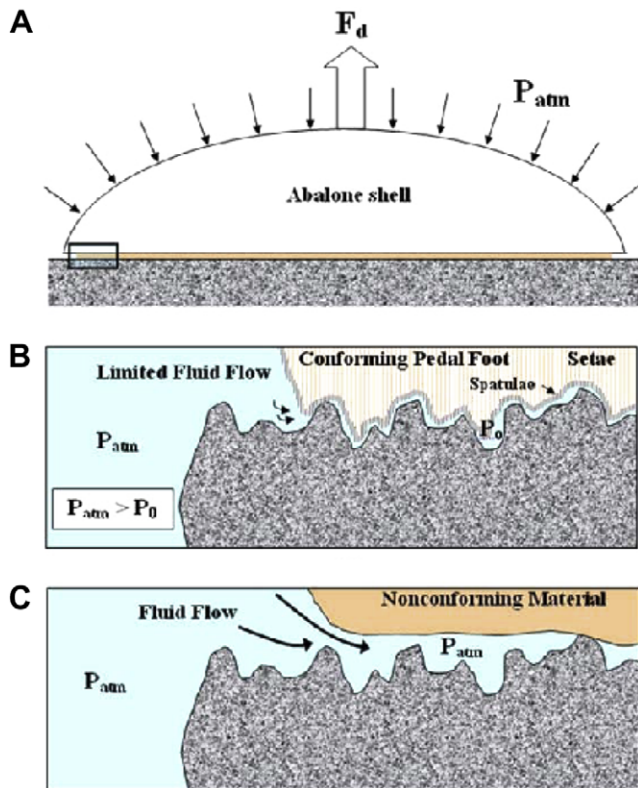


Fig. 10. Schematic diagram of: (A) force balance (the detachment force is equal and opposite to the force created by atmospheric pressure); (B) conforming pedal foot, limiting water flow and (C) non-conforming material, allowing water flow.

decreases. Once it becomes zero, detachment occurs. Fig. 10C shows the situation for a non-conforming material: a continuous fluid path to the interface region ensures pressure equilibration around the animal and effectively eliminates suction. It is proposed that capillarity and van der Waals forces can maintain the intimate contact between the ventral side of the foot pedal and the attachment surface; in this manner the suction force can reach and even exceed $P_{\text{atm}}A$. This is indeed suggested by some of the results presented in Fig. 9, exceeding 101 kPa.

4. Conclusions

Evidence of van der Waals and capillary forces through nanofibrils was observed in the attachment of abalone. SEM shows a structural hierarchy analogous to that of the gecko foot, with setae fibers of approximately $2 \mu\text{m}$ diameter terminating in bundles of nanofibrils uniaxially aligned with individual diameters of approximately 200 nm. The Yao–Gao [33,34] analysis was applied to the fibril terminations, which were found to have a parabolic shape. This enables the application of the JKR equation. Both bulk mechanical test measurements and atomic force measurements show close agreement to theoretical results obtained based on the JKR equation, which predicts a pull-off force of 10 nN for a single nanofibril. Experimental measurements by AFM show a pull-off force of 5 nN per nanofibril from a hydrophobic substrate. Mechanical pull-off measurements showed an average pull-off stress of 115 kPa for abalone with an averaging foot area of $5.5 \times 10^{-3} \text{ m}^2$. AFM testing at different humidity levels shows evidence of capillary effects in combination with van der Waals interactions. Although AFM testing was conducted in an environment below 100% humidity, the results provide insight into the attachment mechanisms applied by the red abalone.

It is justifiable to conjecture that both van der Waals and capillarity forces enable the foot pedal to match different surface profiles so that attachment through suction can be maximized. This ensures survival of the abalone against predatory actions. It is proposed that, as in the case of the gecko, these nanofibrils create intimate contacts at the molecular level to form van der Waals interactions which can be accumulated into a formidable macroscale effect.

Acknowledgements

We thank Professors Eduard Arzt, Joanna McKittrick, Huajian Gao and Lars Bjursten for insightful and inspirational discussions on this topic. Evelyn York at the Scripps Institution of Oceanography and Ryan Anderson at the Nano3 Laboratory in Calit2 are greatly appreciated for assistance with materials characterization. Eddie Kisfaludy provided instrumental assistance with the holding facilities in the Hubbs Hall Laboratory at the Scripps Institution of Oceanography. This research was supported by the National Science Foundation through Grant DMR 0510138.

References

- [1] Autumn K, Liang YA, Hsieh ST, Zesch W, Chan WP, Kenny WT, et al. *Nature* 2000;405:681–5.
- [2] Arzt E, Gorb S, Spolenak R. *Proc Natl Acad Sci* 2003;100:10603–6.
- [3] Autumn K, Sitti M, Liang YA, Peattie AM, Hansen WR, Sponberg S, et al. *Proc Natl Acad Sci* 2002;99:12252–6.
- [4] Gao HJ, Wang X, Yao H, Gorb S, Arzt E. *Mech Mater* 2005;37:275–86.
- [5] Hanna G, Barnes WJP. *J Exp Biol* 1991;155:103–25.
- [6] Barnes WJP. *MRS Bulletin* 2007;32:479–85.
- [7] Scherge M, Gorb S. *Biological micro- and nanotribology: nature's solutions*. Berlin: Springer; 2001.
- [8] Huber G, Mantz H, Spolenak R, Mecke K, Jacobs K, Gorb SN, et al. *Proc Natl Acad Sci USA* 2005;102(45):16293–6.
- [9] Persson BNJ, Gorb S. *J Chem Phys* 2003;119(21):11437.
- [10] Geim AK, Dubonos SV, Grigorieva IV, Novoselov KS, Zhukov AA, Shapoval SYU. *Nat. Mater* 2003;2:461–3.
- [11] Sitti M, Fearing RS. *J Adhes Sci Tech* 2003;17:1055–77.
- [12] del Campo A, Greiner C, Alvarez I, Arzt E. *Adv Mater* 2007;19:1973–7.
- [13] Kim S, Sitti M. *Appl Phys Lett* 2006;89:261911.
- [14] Ge L, Sethi S, Ci L, Ajayan PM, Dhinojwala A. *Proc Natl Acad Sci USA* 2007;104(26):10792–5.
- [15] Lee H, Lee BP, Messerschmid PB. *Nature* 2007;448:338–41.
- [16] Sethi S, Ge L, Ajayan PM, Dhinojwala A. *Nanoletters* 2008.
- [17] Mahdavi A, Ferreira L, Sundback C, Nichol JW, Chan EP, Carter DJD, et al. *PNAS* 2008;105:2307–12.
- [18] Lee J, Majidi C, Schubert B, Fearing RS. *Interface* 2008;5:835.
- [19] Yao H, Rocca GD, Guduru PR, Gao H. *Interface* 2008;5:723.
- [20] Lee J, Fearing RS, Komvopoulos K. *Appl Phys Lett* 2008;93:191910.
- [21] Greiner C, Arzt E, del Campo A. *Adv Mater* 2009;21:479–82.
- [22] del Campo A, Greiner C, Arzt E. *Langmuir* 2007;23:10235–43.
- [23] Varenberg M, Gorb SN. *Adv Mater* 2009;21:483–6.
- [24] Chan EP, Greiner C, Arzt E, Crosby AJ. *MRS Bulletin* 2007;32:496–503.
- [25] Waite JH, Tanzer ML. *Science* 1981;212:1038–40.
- [26] Waite JH. *Int J Adhes Adhes* 1987;7(1):9–14.
- [27] Santos R, Gorb S, Jamar V, Flammang P. *J Exp Biol* 2005;208:2555–67.
- [28] Waite JH, Lichtenegger HC, Stucky GD, Hansma P. *Biochemistry* 2004;43:7653–62.
- [29] Bell EYC, Gosline JM. *J Exp Biol* 1996;199:1005–17.
- [30] Huber G, Gorb SN, Spolenak S, Arzt E. *Biol Lett* 2005;1:2–4.
- [31] Donovan DA, Carefoot TH. *J Exp Biol* 1997;200:1145–53.
- [32] Trueman ER, Hodgson AN. *J Mollus Stud* 1990;56:221–8.
- [33] Gao H, Yao H. *PNAS* 2004;101:7851–6.
- [34] Yao H, Gao H. *J Colloid Interface Sci* 2006;298:564–72.
- [35] Johnson KL, Kendall K, Roberts AD. *Proc Roy Soc London* 1971;324:301–13.
- [36] Derjaguin BV, Muller VM, Toporov YP. *J Colloid Interface Sci* 1975;53:314.
- [37] Maugis D. *J Colloid Interface Sci* 1992;150:243.
- [38] Dugdale DS. *J Mech Phys Solids* 1960;8:100.
- [39] Israelachvili JN. *Intermolecular and surface forces*. 2nd ed. London: Academic Press; 1992.
- [40] French RH. *J Am Ceram Soc* 2000;83:2127–46.